Dabagov
Palumbo

Proceedings of the 51st Workshop of the INFN ELOISATRON Project

CHARGED AND NEUTRAL PARTICLES CHANNELING PHENOMENA

Channeling 2008

Series Editor
A. Zichichi

THE SCIENCE AND CULTURE SERIES — PHYSICS

Series Editor: A. Zichichi

Proceedings of the 51st Workshop
of the INFN ELOISATRON Project

CHARGED AND NEUTRAL PARTICLES CHANNELING PHENOMENA

Channeling 2008

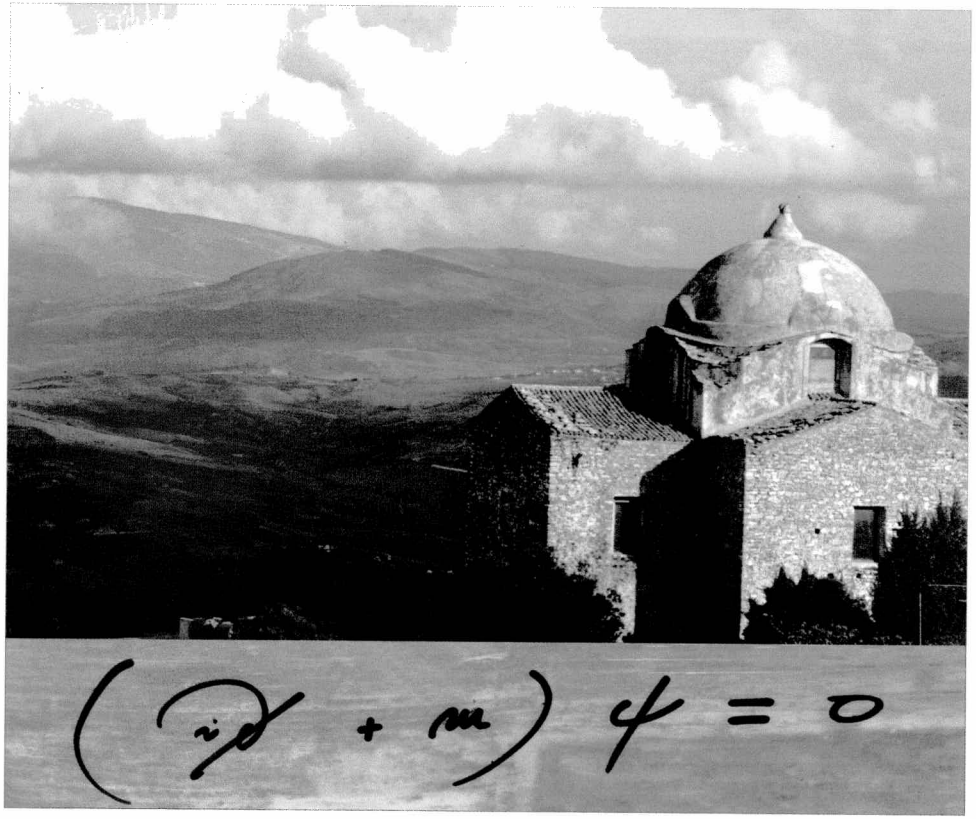

The layout of two additional beam line is sketched in Fig. 5 More information can be found in [15] and in [16]

References

1. L. Palumbo and al., Status of the sparx project, in *Proc. EPAC 2008*, (Genoa, Italy, 2008).
2. A. Cianchi and al., *Phys. Rev. ST-AB* **11** (2008).
3. M. Ferrario and al., *Phys. Rev. Letters* **99** (2007).
4. A. Mostacci and al., *Review of Scientific Instruments* **79** (2008).
5. L. Serafini and J. B. Rosenzweig, *Phys. Rev. E* **55**, p. 7565 (1997).
6. M. Ferrario, HOMDYN Study for the LCLS RF Photo-Injector(march 2000), SLAC-PUB-8400.
7. L. Serafini and M. Ferrario, *Velocity bunching in photo-injectors*, in *AIP Conference Proceedings*, ed. AIP (AIP, 2001).
8. A. Renieri and al., Status report on sparc project, in *Proc. of the 26th FEL Conference*,
9. D. Alesini and al., *NIMA* **568**, 488 (2006).
10. C. Vaccarezza and al., Slice emittance measurements at sparc photoinjector with a rf deflector, in *Proceedings of EPAC 2008*,
11. L. Poletto and al., *1st Technical Design Report for the Seeding @ SPARC experiment*, EUROFEL-Report 2005-DS4-008, Eurofel.
12. O. Tcherbakoff and al., Seeding the sparc test facility with harmonic generation in gases: Preliminary tests of the harmonic generation in gas chamber, in *Proceedings of FEL 2006*,
13. R. Bonifacio and al., *Phys. Rev. Letters* **73** (1994).
14. M. Boscolo and al., *NIMA* **577**, p. 409416 (2007).
15. L. Serafini and al., Compton sources: Physics and applications, following sparc&plasmonx projects, in *Proceedings of Channeling 2008*,
16. D. Giulietti, The status of the plasmonx project, in *Proceedings of Channeling 2008*,

LASER-PLASMA ACCELERATION: FIRST EXPERIMENTAL RESULTS FROM THE PLASMON-X PROJECT

L. A. Gizzi [a,b,e], C.Benedetti[c], S.Betti[a], C.A.Cecchetti[a,e], A.Gamucci[a,b], A.Giulietti[a,b], D.Giulietti[a,b,d,e], P.Koester[a,b,d], L.Labate[a,b], T.Levato[a,b], F.Michienzi[a,d], N.Pathak[a,d], A.Sgattoni[c], G.Turchetti[c], F.Vittori[a,d]

[a] *ILIL, IPCF, Consiglio Nazionale delle Ricerche, Area della Ricerca CNR, Via Moruzzi,1 56124 Pisa, Italy, e-mail l.a.gizzi@ipcf.cnr.it, http://ilil.ipcf.cnr.it*

[b] *INFN, Sez. Pisa, Largo B. Pontecorvo, 3 - 56127 Pisa*

[c] *Universitá di Bologna e Sez. INFN, Bologna, Italy*

[d] *Dipartimento di Fisica "E. fermi, Universitá di Pisa, Italy*

[e] *Laboratori Nazionali di Frascati, INFN, Via E. Fermi, Frascati, Italy*

Bunches of electrons with energy extending up to 10 MeV have been produced using femtosecond laser pulses generated by a sub-2TW, table-top laser system focused on a supersonic gas-jet target. The laser interaction with the gas-jet was studied using a full range of optical, X-ray and γ-ray techniques. The electron bunches were detected using a phosphor screen and a magnetic spectrometer to investigate angular and spectral properties. Our measurements show production of highly collimated electron bunches with moderate energy spread. Also, an experimental configuration exists in which generation of high-charge electron bunches can be obtained with high reproducibility and MeV energies. This regime is investigated in view of its exploitation for applications requiring high average bunch charge and moderate electron energy, including nuclear activation and bio-medical applications.

Keywords: Laser-plasma accèleration, ultrafast laser interactions, multi-MeV electron bunches

1. Introduction

Production of very energetic radiation and particles can be achieved by focusing ultrashort, intense laser pulses onto solids[1] or preformed plasmas.[2] Controlled interaction with gases can lead to the generation of high quality electron bunches exploiting the laser WakeField Acceleration regime (LWFA)[3] that takes advantage of the high electric fields supported in a plasma. In the LWFA the electrons trapped in the plasma wave are ac-

celerated to the phase velocity of the wave that can be very close to the speed of light. Recent experiments,[4–6] and simulations[7–9] show that quasi-monoenergetic electron bunches can be accelerated from the background electron plasma population up to high (>100 MeV) energies, operating in the so-called bubble regime of LWFA. These experiments require a very high laser intensity and typically produce relatively low charge electron bunches.

Recent theoretical works[10] indicate that with a proper choice of laser, plasma, and injection parameters, the acceleration of electron bunches with small energy spread and short bunch length can occur starting from initially large bunch length and energy spread.

By considering that the energy of an accelerated electron bunch can be increased by multiple collinear or non-collinear[11] injections in plasma channels, the stability of the injection and the reduction of the laser energy required for the production of the initial electrons become the key issues of this process. Recently,[12–14] laser-driven electron acceleration at moderate laser intensities (power <10 TW) and application[15] of accelerated bunches to nuclear physics relevant conditions have been demonstrated. Our measurements below show that high accuracy scanning of experimental parameters, including position of beam waist relative to the gas-jet boundary was found to be critical to enable reproducible, multi MeV electron acceleration with a sub-2 TW laser power. We have carried out an experiment to investigate this scenario, searching for the minimum conditions required for a compact, moderate power laser system, to achieve acceleration of electron bunches with high charge and acceptable energy spread for a set of applications.

2. The femtosecond laser source

The Ti:Sa system used in this experiment generates a main pulse of 67 fs duration FWHM with peak power exceeding 2 TW, and a second, lower energy probe with a peak power of 0.1 TW, at the repetition rate of 10 Hz. A schematic view of the entire system is shown in Fig.1.

A Tsunami (Spectra Physics), femtosecond oscillator, pumped by a diode-pumped 5W Nd:YVO CW laser, generates sub-50 fs pulses at a repetition rate of 82 MHz that are stretched and seeded, at a 10 Hz rep rate, into a regenerative amplifier, pumped by a frequency doubled, Nd:YAG, Q-switched laser. After amplification at the 3 mJ level, the stretched pulses are further amplified by a two-pass amplifier pumped by another, frequency doubled, Nd:YAG, Q-switched laser. The output stretched pulse, containing an energy of approximately 15 mJ, is then split in two pulses containing 90% and 10% of the initial energy respectively. The 90% pulse is expanded to a 7 mm diameter beam and compressed using a single grating (folded) compressor to obtain a final pulse duration of less than 65 fs. The remaining 10% pulse is further amplified by a 6-pass amplifier pumped by a frequency doubled Nd:YAG laser delivering 1J pulses at 532 nm, pumping a 2-cm diameter TiSa crystal. The output is further expanded to a 33 mm diameter beam and compressed by a two-grating compressor placed under vacuum. The pulse is compressed to a minimum pulse duration of 67 fs and is then transported under vacuum into the target chamber via two beam steering, motorised turning mirrors, placed in two separate small vacuum chambers.

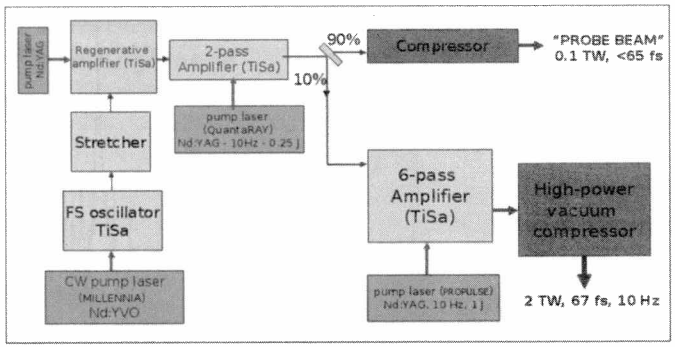

Fig. 1. Schematic diagram of the TW, femtosecond laser system. The main beam is transported to the interaction chamber in vacuum.

The temporal and spatial properties of the femtosecond pulses were characterised in detail using custom developed second-order autocorrelator.[16] The contrast of the laser pulse, i.e. the ratio between the peak power and the low intensity pedestal originating from plepulses and amplified spontaneous emission (ASE) was measured with a third-order cross-correlator (SEQUOIA). In this system, the full power pulse, attenuated by reflections off high quality uncoated glass flats ($\sim 10^2$ attenuation), is split in two equally intense pulses using a beam splitter. One of the pulses is sent through an optical delay line and is frequency doubled in a BBO crystal. The frequeny doubled pulse is combined with the remaining, fundamental pulse in a non-linear crystal to generate third harmonic radiation. The signal is detected in the forward direction by a photomultiplier.

The autocorrelation curve obtained from the second-order autocorrelator yielded a laser pulse duration (FWHM) of 67 fs. The cross-correlation curve over a range of 200 ps is shown in Fig.2. The plot clearly shows a contrast

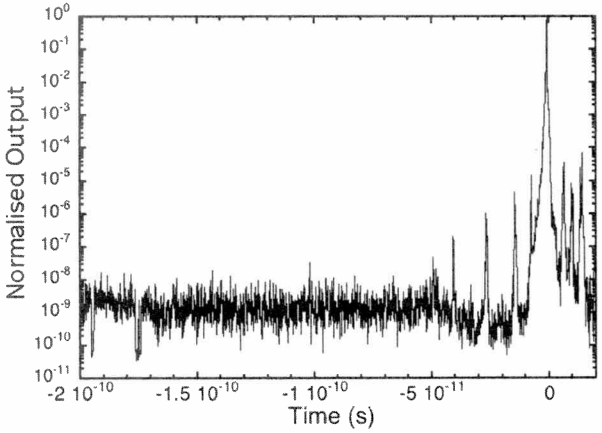

Fig. 2. Cross-correlation curves showing the laser pulse and the detailed structure of the laser pulse in the 200 ps window before the main pulse.

of 10^9 over the entire explored range. Moreover, the intensity of the short prepulses before the main pulse is below 10^{-5} times the intensity of the main pulse. According to these measurements, our laser system can be considered basically free from pre-pulse. This was further verified by interferometry measurements taken at different time-steps around the main pulse, showing no detectable plasma formation up to a few tens of femtoseconds before the main pulse. The spatial quality of the laser pulse was studied by means of an equivalent plane monitor (EPM) using a 100 cm nominal focal length optics and a 12 bits CCD camera (a Photometrics Sensys) with a pixel size of 8 μm size. These EPM measurements show that with the 20 cm focal length off axis parabolic mirror used in our experiment, a FWHM focal spot of approx. 10 μm is found containing a large fraction (up to 90%) of the laser pulse energy. Considering the pulselength of 67 fs and an energy of 120 mJ we find that the maximum intensity on the target can exceed $10^{18} W/cm^2$.

3. The experimental setup

In the experiment, the main pulse was focused onto a gas-jet target using an F/6 off-axis parabola. The gas-jet target was irradiated at full laser energy varying the gas backing pressure, i.e. the pressure in the pipe before the fast valve controlling the nozzle to change the value of the maximum density of the neutral gas. Two gases were used in our experiment, namely He or N_2.

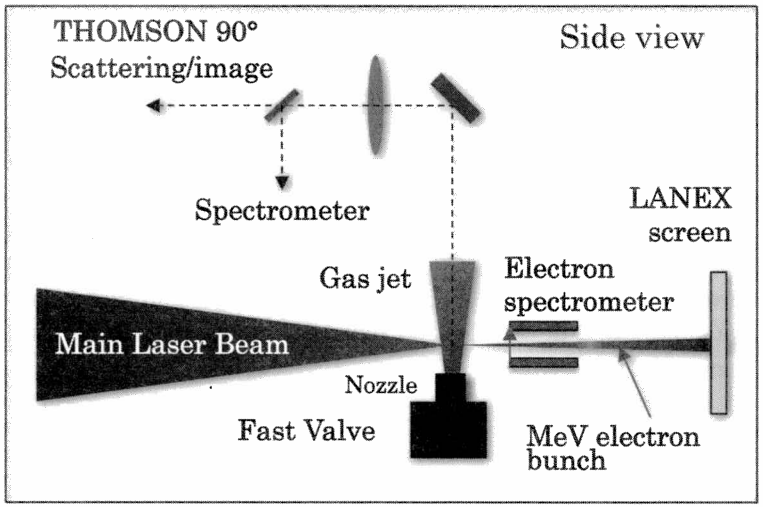

Fig. 3. Schematic layout of the experimental setup: side view showing the main interaction geometry of the laser beam relative to the gas-jet, the magnetic electron spectrometer and the LANEX screen for detection of electrons.

Characterisation of the neutral gas was carried out using optical interferometry. The use of two gases He and N_2, enabled us to explore targets characterised by different physical properties mainly related to the atomic number, and, in particular, to the ionization properties under irradiation of ultrashort, intense laser pulses. The gas-jet nozzle was characterised by a 4 mm long, 1.2 mm wide slit and was mounted on a micrometric motorized support in order to move the interaction point along the three cartesian axes (position scan). During the pulsed operation, the gas flows out of the slit at supersonic speed in order to produce steep interfaces between gas and vacuum. The vacuum in the chamber before the shot is mantained at a pressure below $\sim 10^{-4}$ Torr by a turbo-molecular pump (Varian Turbo-V 550) connected to the chamber by a gate-valve.

A full scan of the position of the focal plane along the laser propagation axis and with respect to the top of the nozzle was performed to find the best conditions for acceleration. An important feature consistently observed throughout the experiment is that electron acceleration in our experimental conditions was always found to occur when the focal plane (waist) was located in the proximity of the near edge of the nozzle, tipically at ~ 0.6 mm from the top of the nozzle. A full scan in pressure was also performed, showing that at higher pressure more stable, but less collimated electron

bunches are produced.

Several diagnostics were used to study the laser-target interaction and the accelerated electrons as shown schematically in Fig.3. Thomson scattering and Nomarski interferometry were set up perpendicularly to the main laser pulse propagation axis to study and characterize ionisation and basic laser-plasma interaction issues. A second group of diagnostics including scintillators coupled to photomultipliers, a phosphor screen (LANEX), an electron spectrometer based upon permanent magnets and dose sensitive, radiochromic film stacks (SHEEBA), enabled indirect and direct detection and characterization of the electron bunches accelerated during the laser-gas interaction.

4. Thomson scattering

Thomson scattering diagnostic was used throughout the experiment to monitor interaction conditions and to identify the basic plasma parameters. In the classical picture of Thomson scattering, the electrons oscillate in the laser field and, in turn, emit radiation. The properties of this scattered radiation are thus related to the properties of the medium. The particle will move mainly along the direction of the oscillating electric field, resulting in electromagnetic dipole radiation. The scattering can be described in terms of the emission coefficient defined as ϵ where $\epsilon dt dV d\Omega d\lambda$ is the energy scattered by a volume element dV in time dt into solid angle $d\Omega$ between wavelengths λ and $\lambda + d\lambda$.
In our case, with the diagnostic placed perpendicularly to the plane in which the laser field oscillates, the emission coefficient can be written:

$$\epsilon = \frac{\pi\sigma}{2} I n_e \tag{1}$$

where σ is the Thomson differential cross section, n_e is the electron density, and I is the incident flux.

This result simply shows that the Thomson scattering provides combined information on the laser intensity and electron density. Since in our case, knowledge on the plasma density can be derived independently from the plasma interferometry, we can use Thomson scattering to derive information on the laser intensity. In our experimental set up an F/10 achromatic doublet was used to produce a 10X magnified image of the interaction region.

The image of Fig.4 shows an overview of the emission produced along the entire laser propagation axis. The waist of the laser beam is placed on the edge of the gas-jet (dashed line in the image) and Thomson scattering

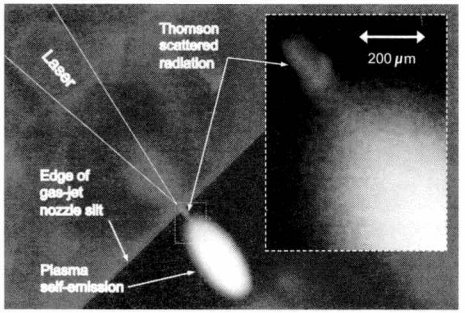

Fig. 4. Typical top-view image of the gas-jet nozzle obtained by the Thomson scattering diagnostic channel showing the main features of the interaction. The waist of the laser beam is placed on the edge of the gas-jet where Thomson scattering radiation is clearly visible (red in colour image). Beyond that point, the laser beam expands and the emission visible in the image is dominated by white light plasma self-emission. The insert in the top-right side of the image shows the magnified region of interaction

radiation is clearly visible as a $\sim 200\mu m$ long channel-like structure. Beyond that point, the laser beam expands and the emission visible in the image is dominated by plasma self-emission. We observe that the length of the channel is approximately twice the expected depth of focus (Rayleigh length) of 100 μm. This observation suggest that a laser pulse channeling is taking place which significantly extends the length of the interaction region. This observation is confirmed by the interferometry measurements presented below. Also visible in the magnified insert of Fig.4 is the detailed structure of the Thomson scattering emission along the laser propagation direction. In some shots, a periodicity ranging from 14 to 20 μm was observed and in some cases, blue shifted emission up to approximately 500 nm was associated to this region. These circumstances are being investigated to identify a possible role of the electron plasma wave in the structure of the emitting region in the Thomson scattering image.

5. Optical interferometry

As anticipated above, a Nomarski interferometer (see[17] and references therein) was arranged with the line of sight set to be perpendicular to the main laser pulse propagation axis to study plasma formation and evolution. It is well known that optical probing technique is based upon the dependence of the plasma refractive index on the electron density:

$$\eta = \sqrt{1 - \frac{n_e}{n_c}} \backsimeq 1 - \frac{n_e}{2n_c}. \tag{2}$$

In the Nomarski interferometer, a probe beam is set to propagate through the region of interest. A lens is used to image the region of interest with the required magnification and resolution. A Wollaston prism is then used to splits the probe beam into two partially overlapping beams. In the overlapping region an interference pattern is produced with a fringe separation that can be modified by changing the position of the Wollaston prism relative to the lens. In our experiment, the fringes were set to be perpendicular to the laser propagation direction.

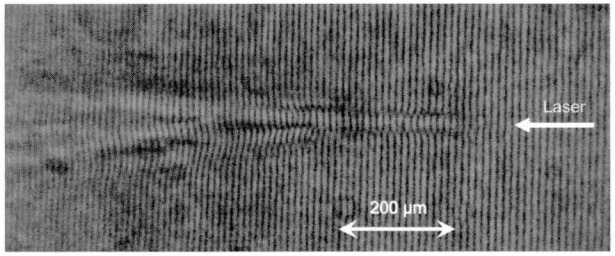

Fig. 5. Interferogram of the gas-jet interaction region taken 2 ps after propagation of the laser pulse. The shot was taken in N_2 at a backing pressure of 35 bar, with the laser focal plane located 50 μm into the gasjet and 400 μm from the nozzle output plane.

Fig.5 shows a typical interferogram taken after propagation throughout the gas-jet. This image clearly shows a collimated propagation of the laser pulse over a distance of approximately 200 μm. Beyond this point, the beam rapidly expands with a clear evidence of beam break-up and filamentation. The extraction of the electron density from the interferogram was performed using the code IACRE[18,19] . The density map thus obtained shows a maximum electron density of $7 \times 10^{19} cm^{-3}$ in the 200 μm long plasma channel.

6. Electron beam characterisation

As already pointed out above, we stress that electron acceleration in our experiment was only found to occur when the laser beam waits was located in the proximity of the edge of the nozzle, typically within a few hundreds of μm. Also, electron bunch production was rapidly fading when the distance of the waist from the output plane of the gas-jet nozzle slit was more that 800 mum. In our case, due to laser beam and nozzle geometry, the minimum possible distance was $\sim$ 0.6 mm to avoid laser damage of the nozzle tip.

In this section we show the results of characterization of the laser accelerated electrons. For these mesaurements four different diagnostics were used for different purposes. A set of 3 scintillators were arranged to detect the γ-rays produced by the electrons via bremsstrahlung on the target chamber. A phosphor screen (Kodak LANEX Regular Screen) was placed on the laser axis to image out the accelerated electron beam. The dosimetric film stack (SHEEBA), based upon Radiochromic films[20] was used to obtain independent spectro-angular distribution of electrons.

In the case of scintillators, the scattering of energetic electrons within the walls of the chamber generates γ-ray which can be detected and measured by an oscilloscope. Two scintillator detectors with different thickness of the active material (NaI) of 52 mm and 25 mm, shielded by a 5 mm thick layer of Pb, were placed along the laser propagation axis. A third detector, with a 12 mm thick NaI and without shielding, was placed perpendicularly to the mentioned direction to detect radiation propagating off-axis. The signal was recorded by a multi-channel oscilloscope. This diagnostic enable us to monitor the best conditions for electron acceleration in terms of reproducibility of the signal. The LANEX phosphor screen was filtered with a 25 μm Al foil and was coupled with an optical system imaging its rear surface. When an electron hits the sensitive material as shown in Fig. 3, the phosphors emit optical (green) radiation from the rear surface of the screen. This radiation was then imaged out of the vacuum chamber using a photographic objective, on to a commercial digital SLR camera (Pentax Digital Camera K 100D Super). The camera was equipped with a custom built trigger unit to enable synchronized shooting with the shortest possible shutter operation of 250 ms. This set up enabled direct observation of the electron bunch divergence and allowed us to obtain information on the shot by shot fluctuations of the bunch charge.

Fig.6 shows a raw image of the entire exposed LANEX area, with the electron beam pattern obtained in two shots taken in two different experimental conditions. Fig.6a) presents the typical electron signal from N_2 gas (@50 bar backing pressure) that shows a large bunch divergence of approximately 20 degrees. A much narrower angular distribution is found in the case of He gas (@ 50 bar) shown in fig. 6b) which is of the order of 2 degrees (FWHM). While the narrow beam condition was not highly reproducible, the beam pattern of Fig.6a) was very stable and reproducible, in a range of pressures from 30 to 40 MeV. In these experimental conditions, our system becomes a potentially interesting tool for applications of high-charge electron beams.[15]

A spectral analysis of the accelerated electrons was carried out using

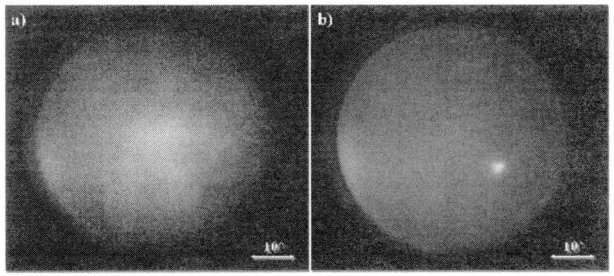

Fig. 6. Typical outputs of LANEX in detection configuration. a) non collimated laser-accelerated electrons in case of N_2 gas @ 50 bar. b) collimated laser-accelerated electron bunch in case of He gas @ 50 bar.

a magnetic spectrometer coupled with the LANEX screen. The spectrometer, based upon permanent NeFeB magnets generating a quasi-uniform magnetic field (BMax $\sim$ 0.45 T), was placed at a distance of 44 mm in front of the LANEX screen. The magnetic field amplitude was mapped in the region of interest using a millimeter-sized Hall magnetic probe. A 2 mm thick Pb foil with a $\sim$ 0.5 mm slit width was placed in front of the magnet, with the slit direction parallel to the magnetic field, in order to limit the transverse momentum of electrons accepted by the electron spectrometer and consequently to increase the resolution of the spectrometer.

Numerical modelling[21] based upon particle tracing in the mapped magnetic field was implemented to describe the performance of the spectrometer In order to obtain the dispersion curve and the intrinsic resolution of both the imaging acquisition system and the LANEX screen. The code also account for errors introduced by beam pointing instability and space-charge effects along propagation. The results obtained by the magnetic spectrometer were confirmed by independent measurements carried out using and energy spectrometer consisting of sandwiched Radiochromic films[22] (RCF). A sample spectrum obtained with the magnetic spectrometer with N_2 gas-jet is displayed in Fig.7.

According to this spectrum, electrons up to 10 MeV were detected, with an overall spectral distribution characterized by a broad peak with a maximum between 5 and 6 MeV. In some shots, narrower spectral components were found, thought with a poor reproducibility. A summary of the results obtained in our experimental condition and for both He and N_2 gas-jet is reported in Table 1. Also included in the table is a list of the main parameters characterizing our experimental set up, including laser and gas-jet parameters. These results confirm that, in spite of the very low laser intensity compared with most of the experiments available in literature, the electrons accelerated in our experimental conditions are well in the multi-MeV region, with evidence of mono-energetic components emerging clearly from the broad energy spectrum. Remarkably, a stable production of electron bunches was obtained when using the N_2 gas-jet, while the use of He resulted in a less reproducible operation, with narrower beam divergence.

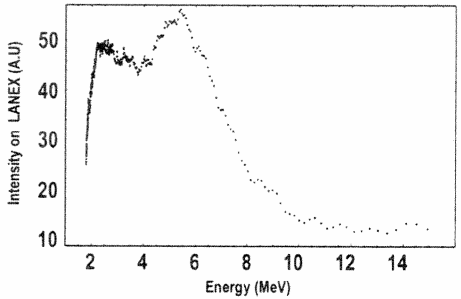

Fig. 7. Electron spectrum obtained with the magnetic spectrometer showing quasi monoenergetic peak between 5 and 6 MeV. The spectrum was obtained from irradiation of a N_2 gas-jet at a backing pressure of 45 bar

Table 1. Experiment parameters table

Input paramenters	Output parameters
Laser wavelength= 800 nm	$n_e = 7 \times 10^{19} cm^{-3}$
Laser pulse duration $\geq$ 65 fs	Plasma channel length $\approx$ 200 μm
Laser energy$<$ 120 mj	Plasma channel diameter $\leq$ 30 μm
Optics numerical aperture = F/6	Max energy (cut-off)$\approx$ 10 MeV
Calc. focal spot radius = 3 μm	Electron energy peak @ 5-6 MeV
Calc. depth of focus = 24 μm	e-beam divergence (He) $<$ 3deg
Meas. focal spot diam.= 10 μm	e-beam divergence (N_2)$\approx$ 10deg
gas-jet thickness = 1.2 mm	e-beam reproducibility (N_2): high
	Bunch charge (N_2) $>$ 0.1nC

The control of these features is a very complex task that requires an accurate knowledge of the key parameters of our experimental configuration and the identification of the main acceleration mechanism occurring in our experiment. Starting from the assumption that wakefield acceleration is the basic mechanism behind our results, we explored this possible scenario using the Particle-in-Cell numerical code AlaDyn[23] capable of modelling a 3-dimensional laser-plasma interaction configuration. ALaDyn is a fully self-consistent, 1/2/3D, relativistic Electro-Magnetic PIC code capable of

handling laser pulse(s), injected bunch(es) and a user defined plasma, featuring high order schemes in space/time, with computational moving window, stretched computational grid and Boosted Lorentz frame. This code enabled us to take into account details of our experimental configuration, including laser parameters, focusing geometry and some of the gas-jet features.

7. Discussion

A first crucial observation that arises from simple considerations on our experimental set up is that a significant laser beam self-focusing may occur in our experimental conditions. According to the well known expression for relativistic self-focusing, $P_{cr} \approx 17(\omega/\omega_p)^2$ GW and taking into account the measured electron density of $7 \times 10^{19}\text{cm}^{-3}$, we find that the critical power in our experimental conditions is 0.4 TW, which is well below the nominal power of our laser system. This result suggests that in our experiment, conditions are satisfied for laser beam self-focusing to occur. A confirmation of this result was obtained from 3-dimensional AlaDyn calculations as summarised in the plot of Fig.8, that shows the evolution of the laser beam intensity along the propagation distance. Two different density profiles have been considered in order to keep into account shot-to-shot variability and to study the sensitivity of the dynamics to the physical parameters.

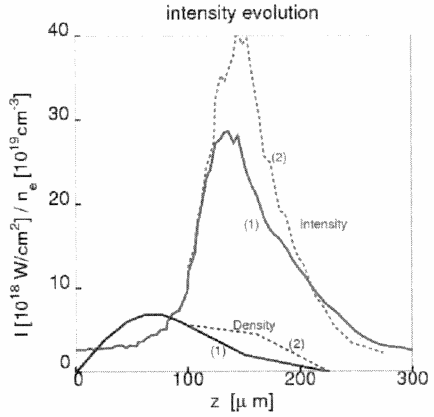

Fig. 8. Evolution of the beam intensity (in red) showing that in our experimental conditions a strong self-focusing occurs on a longitudinal scalelength of less than 100 μm, leading to a more than 10-fold increase of the local intensity. The solid and dashed lines refer respectively to the density profiles #1 and #2.

In both cases, according to the simulations, the self-focusing brings the peak laser beam intensity up to a value larger than 2.7×10^{19} W/cm^2. The ponderomotive force associated with the leading front of this very high intensity pulse leads to a strong charge separation with the consequent growth of electron plasma waves. We observe the formation of a main wake with a "bubble"-like[24] structure (see Fig.9). Even if the normalised vector potential of the laser ($a = eA/mc^2$) reaches the peak value $a \simeq 4$ which would be compatible with particle injection in the bubble regime,[25,26] we do not observe injection from the rear side of the bubble. This is due to the fact that the decreasing plasma ramp (see Fig.8) is unable to sustain the self-focusing over a long distance and the laser intensity suddenly drops (on a scale of $\sim$ 50 μm) to values which are unfavorable to the injection. However, trapping of the background particle inside the wake is possible. These particles are accelerated up to energies of 15-20 MeV and exhibit an

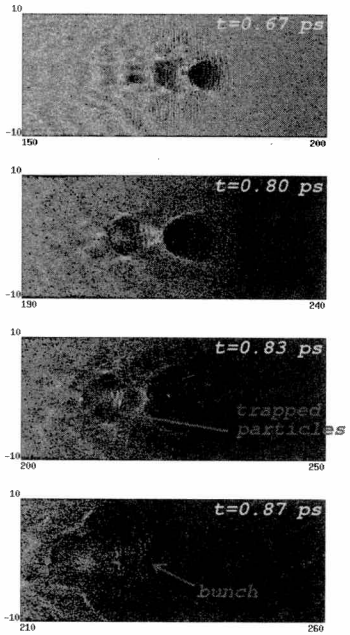

Fig. 9. Electron density cut at different times, as obtained from PIC simulation, showing the growth of the wake-field structure. The observation window of the code moves at the speed of light following the laser propagation. Electron density increases from blue to red.

overall thermal-like spectrum since they interact with the transverse field of

the laser pulse whose length ($\gtrsim 20$ μm) is larger compared to the "bubble" size which is of the order of the plasma wavelength ($\sim 5 \div 10$ μm). According to the PIC simulations the accelerated charge is approximately ~ 0.1 nC (in agreement with experimental data) and the angular divergence of the beam is in the range $10^o \div 16^o$ (FWHM).

An additional interesting observation concerning the accelerated bunch is the longitudinal modulation of the bunch density induced by the interaction of the bunch itself with the longitudinal component of the co-propagating laser beam.[27,28] As shown in the three-dymensional plot of

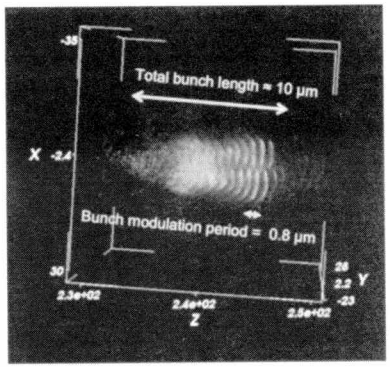

Fig. 10. Accelerated bunch at the exit of the plasma as obtained from AlaDyn PIC simulation. The modulation of the accelerated electron bunch is due to the interaction with the longitudinal electric field component of the co-propagating linearly polarised laser pulse.

Fig.10, the total bunch length exiting the interaction region is expected to be approximately 10μm, with the leading edge clearly showing the effects of the charge modulation with the characteristic wavelength of the laser radiation (0.8 μm), corresponding to a modulation period of less than 3 fs.

In the experiment, interaction of the accelerated electrons with the plasma and with the mm-sized remaining plasma and/or ionized gas is likely to modify the spectral distribution, possibly depleting the lower energy end of the distribution as predicted by simulations. Also, the spectral properties of the accelerated bunch are expected to depend critically upon the trapping process. Given the strong influence of self-focusing in the formation and the dynamics of the accelerating cavity, we may expect that the trapping process may also be influenced in our experimental conditions. Therefore, on the basis of the modeling performed so far, no conclusion can yet be reached on the possible origin of the mono-energetic components

observed in our measurements and further modeling is being performed to identify the key parameters for the onset of trapping conditions.

8. Conclusions

We presented the recent results obtained in the frame of the PlasMonX collaboration, on laser acceleration of electrons with self-injection using the sub-2TW ILIL femtosecond laser system. High accuracy scanning of experimental parameters, including position of beam waist relative to the gas-jet boundary was found to be critical to enable self-injection. Conditions were identified yielding higher charge (in N_2 gas-jet) or higher quality (in He gas-jet) electron bunches, with acceleration gradients greater than 50 GeV/m. Evidence on non-thermal electron spectrum with a mono-energetic component with a 20% energy spread above 5 MeV was found. Numerical simulations show that in our experimental conditions occurrence of strong self-focusing is expected, leading to an enhancement of the local laser intensity well above 10^{19} W/cm^2, with the activation of a single acceleration cavity, resembling the so-called "bubble"-like regime. Our optical data show that an important role in the experiment was played by the very high contrast of our femtosecond laser pulse that enables clean interaction of the femtosecond laser pulse with the field-ionised gas medium, without prior plasma formation. We are now ready to explore[29] this acceleration regime using the much brighter FLAME laser, that will allow a much longer depth of focus of a few mm to be used, extending the accelerating length over the entire gas medium.

9. Acknowledgements

This work was partially supported by the INFN Project Plasmon-X and by the MIUR funded FIRB-SPARX project and by the MIUR-PRIN project Studio della Generazione e della propagazione di elettroni rapidi [...]". We would like to thank W. Baldeschi, A. Barbini, A. Rossi and M. Voliani of the IPCF-CNR staff for their invaluable technical assistance. We acknowledge the support of the CINECA for the simulations (grant "Simulazioni PIC 3D per l'accelerazione laser-plasma").

References

1. L. A. Gizzi, D. Giulietti, A. Giulietti, P. Audebert, S. Bastiani, J. P. Geindre, and A. Mysyrowicz. Simultaneous measurements of hard X-rays and second-harmonic emission in fs laser-target interactions. *Physical Review Letters*, 76(13):2278, March 1996.

2. D. Giulietti, M. Galimberti, A. Giulietti, L. A. Gizzi, P. Tomassini, M. Borghesi, V. Malka, S. Fritzler, M. Pittman, and K. Taphouc. Production of ultra-collimated bunches of multi-mev electrons by 35-fs laser pulses propagating in exploding-foil plasmas. *Physics of Plasmas*, 9:3655, 2002. letter.
3. T.Tajima and J.M.Dawson. Laser electron accelerator. *Physical Review Letters*, 43(4):267, July 1979.
4. J. Faure, Y. Glinec, and A. Pukhov et al. A laser-plasma accelerator producing monoenergetic electron beams. *Letters to Nature*, 431:541, September 2004.
5. V. Malka, J. Faure, , and Y. Glinec et al. Monoenergetic electron beam optimization in the bubble regime. *Phys.Plasmas*, 12:056702, January 2005.
6. J.Faure, Y.Glinec, and G.Gallot et al. Ultrashort laser pulses and ultrashort electron bunches generated in relativistic laser-plasma interaction. *Phys.Plasmas*, 13:056706, February 2006.
7. A.Pukhov, S.Kilesev, and I.Kostyukhov et al. Relativistic laser plasma bubbles: new sources of energetic particles and x-rays. *Nucl.Fusion*, 44:S191–S201, December 2004.
8. A.Pukhov, S.Gordienko, and S.Kilesev et al. The bubble regime of laser-plasma acceleration: monoenergetic electrons and the scalability. *Plasma Phys. Control. Fusion*, 46:B179–B186, 2004.
9. I.Kostyukhov, A.Pukhov, and S.Kilesev. Phenomenological theory of laser-plasma interaction in "bubble" regime. *Phys.Plasmas*, 11:5256, November 2004.
10. D. F. Gordon, R. F. Hubbard, and J. H. Cooley et al. Quasimonoenergetic electrons from unphased injection into channel guided laser wakefield accelerators. *Physical Review E*, page 026404, February 2005.
11. D. Kaganovich, D. F. Gordon, and A. Ting. Observation of large-angle quasimonoenergetic electrons from a laser wakefield. *Phys.Rev.Lett*, 100:215002, May 2008.
12. B. Hidding, K. Amthor, B. Liesfeld, H. Schwoerer, S. Karsch, M. Geissler, L. Veisz, K. Schmid, J. Gallacher, S. Jamison, D. Jaroszynski, G. Pretzler, and R. Sauerbrey. Generation of quasimonoenergetic electron bunches with 80-fs laser pulses. *Phys.Rev.Lett*, 96:105004, 2006.
13. K. Koyama, M. Adachi, E. Miura, S. Kato, S. Masuda, T. Watanabe, A. Ogata, and M. Tanimoto. Monoenergetic electron beam generation from a laser-plasma accelerator. *Laser and Particle Beams*, 24:95–100, 2006.
14. A. Masuda, E. Miura, K. Koyama, S. Kato, M. Adachi, T. Watanabe, K. Torii, and M. Tanimoto. Energy scaling of monoenergetic electron beams generated by the laser-driven plasma based accelerator. *Phys.Plasmas*, 14:023103, 2007.
15. A Giulietti, N Bourgeois, T Ceccotti, X Davoine, S Dobosz, P D'Oliveira, M Galimberti, J Galy, A Gamucci, D Giulietti, LA Gizzi, DJ Hamilton, E Lefebvre, L Labate, JR Marquès, P Monot, H Popescu, F Réau, G Sarri, P Tomassini, and P Martin. Intense gamma-ray source in the giant-dipole-resonance range driven by 10-tw laser pulses. *Phys.Rev.Lett*, 105002, 2008.
16. M.Galimberti. Realizzazione di un autocorrelatore a singolo impulso a dye.

Technical Report 1/122002, IPCF-CNR Pisa, Dicember 2002.
17. L.A.Gizzi, D.Giulietti, and A.Giulietti et al. Characterization of laser plasmas for interaction studies. *Phys.Rev.E*, 49(6):5628, June 1994.
18. P.Tomassini and A.Giulietti. A generalization of abel inversion to non-axisymmetric density distribution. *Optics Communications*, 199:143–148, November 2001.
19. Paolo Tomassini, Antonio Giulietti, and Leonida A. Gizzi et al. Analyzing laser plasma interferograms with a continuous wavelet transform ridge extraction technique: the method. *Appl.Opt.*, 40(35):6561, December 2001.
20. E. Breschi, M. Borghesi, M.Galimberti, D. Giulietti, L.A. Gizzi, and L. Romagnani. A new algorithm for spectral and spatial reconstruction of proton beams from dosimetric measurements,. *NUCLEAR INSTRUMENTS & METHODS IN PHYSICS RESEARCH SECTION A-ACCELERATORS SPECTROMETERS DETECTORS AND ASSOCIATED EQUIPMENT*, 522:190, 2004.
21. F.Vittori. Analisi dati con specmag. Technical report, IPCF-CNR Pisa, September 2008.
22. Marco Galimberti, Antonio Giulietti, and Danilo Giulietti et al. Sheeba: A spatial high energy electron beam analyzer. *Rev.Sci.Inst.*, 76:053303, April 2005.
23. C. Benedetti, A. Sgattoni, G. Turchetti, and P. Londrillo. Aladyn: A high-accuracy pic code for the maxwell–vlasov equations. *Plasma Science, IEEE Transactions on*, 36:1790, 2008.
24. A. Pukhov and J.Meyer ter Vehn. Laser wake field acceleration: The highly non-linear broken-wave regime. *Appl. Phys. B*, 74:355–361, 2002.
25. S.P.D. Mangles, A.G.R. Thomas, C. Bellei, A.E. Dangor, C. Kamperidis, S. Kneip, S.R. Nagel, L. Willingale, and Z. Najmudin. Self-guided wakefield experiments driven by petawatt-class ultrashort laser pulses. *Plasma Science, IEEE Transactions on*, 36:1715, 2008.
26. M. Geissler, J. Schreiber, and J. Meyer ter Vehn. Bubble acceleration of electrons with few-cycle laser pulses. *New Journal of Physics*, 8:186, 2006.
27. Melvin Lax, William H. Louisell, and William B. McKnight. From maxwell to paraxial wave optics. *Phys.Rev.A*, 11:1365, 1975.
28. L. Cicchitelli, H. Hora, and R. Postle. Longitudinal field components for laser beams in vacuum. *Phys.Rev.A*, 41:3727, 1990.
29. L. A. Gizzi, A. Bacci, S. Betti, C.A. Cecchetti, M. Ferrario, A. Gamucci, A. Giulietti, D. Giulietti, P. Koester, L. Labate, T. Levato, V. Petrillo, L. Serafini, P. Tomassini, and C. Vaccarezza. An integrated approach to ultraintense laser sciences: the plasmon-x project. *Europ. Phys. Journal - Special Topics*, 2009. in press.